International Journal of Automotive Technology, Vol. 16, No. 3, pp. 427–433 (2015)
DOI 10.1007/s12239–015–0044–z

Copyright © 2015 KSAE/ 084–08
pISSN 1229–9138/ eISSN 1976–3832

ESTIMATION OF LATERAL DISTURBANCE UNDER PARAMETER UNCERTAINTIES

K. W. KIM[1], S. B. LEE[2], C. S. PARK[2] and K. YI[1]*

[1]School of Mechanical and Aerospace Engineering, Seoul National University, Seoul 151-742, Korea
[2]Steering Software Design Division, Hyundai Mobis, 17-2 Mabuk-ro, 240 Beon-gil, Giheung-gu, Yongin-si, Gyeonggi 446-912, Korea

(Received 4 October 2013; Revised 17 June 2014; Accepted 19 June 2014)

ABSTRACT–This paper presents a lateral disturbance estimator based on Motor Driven Power Steering (MDPS)-based driving assistant system considering parameter uncertainties. A vehicle motion can be laterally deviated by lateral disturbance including wind force and load from bank angle. MDPS systems using motors to assist steering torque have become common in production vehicles. The motor-assisted torque can be controlled by the motor overlay torque within a physically feasible range. To determine MDPS motor overlay torque for compensating lateral disturbance, the information of lateral disturbance is necessary and estimated data was used due to measurement difficulties. The proposed estimator includes a tire self-aligning torque estimator based on Kalman filter with a 2-degree-of freedom (2-DOF) bicycle model. A simulation study was conducted to analyze the influence of parameter variation and to investigate the appropriate parameters under various load conditions. The performance of the proposed estimator considering the vehicle parameter uncertainties has been evaluated for several levels of the lateral disturbances. The estimation algorithm has been evaluated via closed-loop simulation and test data.

KEY WORDS : Lateral disturbance, Crosswind, Bank angle, Kalman filter, MDPS, Estimation, Parameter uncertainty

NOMENCLATURE

$F_{CW,i}$: crosswind force of i-axis
$C_{f,i}$: coefficient of crosswind force
ρ : air density
$C_{f,i}$: coefficient of crosswind force
v_r : wind velocity relative to vehicle
A : vehicle frontal area
$M_{CW,i}$: crosswind moment of i-axis
$C_{n,i}$: coefficient of crosswind moment
l : wheel base
v_x : vehicle longitudinal speed
v_{CW} : crosswind speed
ψ : yaw angle
β_{CW} : airflow side slip angle
$F_{yfr/l}$: front lateral tire force of right/left tire
$F_{xfr/l}$: front longi tire force of right/left tire
$F_{yrr/l}$: rear lateral tire force of right/left tire
$F_{xrr/l}$: rear longi tire force of right/left tire
F_{CW} : crosswind force
θ : crosswind angle of attack
d : vehicle tread width
T_{align} : self-aligning torque of i-th tire
t_f : half tread width
l_f : distance between the c.g and front wheel axis
l_r : distance between the c.g and rear wheel axis
F_{BANK} : lateral force due to bank angle
m : vehicle mass
g : acceleration of gravity
Δz : height difference of left/right tire
β : vehicle body side slip angle
γ : vehicle yaw rate
$\alpha_{f/r}$: tire slip angle of front/rear tire
$F_{f/r}$: front/rear tire force
$C_{f/r}$: cornering stiffness of front/rear tire
J : inertia of steering
N : steering gear ratio
T_{column} : steering column torque
T_{assist} : motor assist torque
T_{SAT} : sum of the self-aligning torque of front tires
$T_{friction}$: friction torque
K : proportional rate of the self-aligning torque
F_W : lateral force due to lateral disturbance
M_W : yaw moment due to lateral disturbance
δ_f : front steering angle
ϕ : vehicle roll angle
ϕ_{BANK} : additive roll angle due to bank angle
F_{zi} : vertical tire force of i-th tire

*Corresponding author. e-mail: kyi@snu.ac.kr

1. INTRODUCTION

Lateral disturbances lead a vehicle deviate from the desired

path against its driver's intention. The major sources of lateral disturbances are considered as crosswind on bridges or near sea shores and road bank angle. The lateral disturbance by crosswind is negligible if the vehicle is moving low speed. However, in the high speed or strong crosswind, it may cause unintended lane departure or rollover. The previous research revealed that the lateral disturbance from the crosswind may lead the vehicle deviate from its path enough to cause an accident (Baker, 1986). The lateral load from bank angle also causes the unwanted leaning motion toward the direction of the load. The lateral disturbance from the crosswind or bank angle may reduce the driver's refinement in driving situation.

In recent years, Motor Driven Power Steering (MDPS) system, which uses a motor to assist the steering torque, has become common in production vehicles. MDPS system is expected to be an alternative system to replace the conventional hydraulic steering system. The sensors of MDPS can measure steering torque, motor assist torque, steering column velocity, and steering angle. Since the worldwide mass production of MDPS is expected, an estimator using MDPS sensor signal can be easily applicable to vehicles equipped with it. A previous research for estimating the wind disturbance used a vision sensor on high class vehicle which is less common (Glaser *et al.*, 2008).

In this paper, the estimator for lateral disturbance has been proposed. It is possible to estimate lateral disturbance without any additional sensors such as a vision sensor, and for the better performance of the estimation, the appropriate parameters have been investigated through the simulation studies using MATLAB/Simulink and CARSIM. The vehicle parameter uncertainties in various load conditions have been considered, and those effects on the proposed estimation algorithm have been evaluated.

This paper is organized as follows. Section 2 describes the vehicle simulation model which has been validated with the actual test data. Lateral disturbance model is presented in section 3, and the detail design procedure of lateral disturbance estimator is described in section 4.

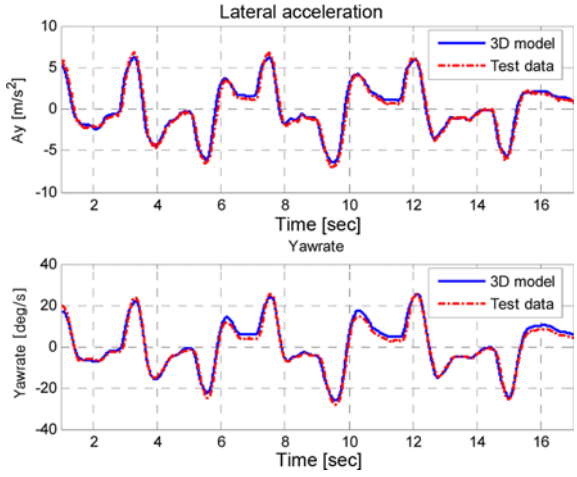

Figure 1. Lateral behavior validation with test data.

2. VEHICLE MODEL

In order to apply lateral load dynamics, a vehicle simulation model has been developed. The vehicle simulation model has been developed with MATLAB/Simulink software. The vehicle model is consisted of 6-DOF sprung mass and 4-quarter car models for investigating vehicle body dynamics (Ha *et al.*, 2003). The Magic formula tire model is used to represent the vehicle longitudinal, lateral and vertical motion. Hyundai YF Sonata F24 has been chosen as the target vehicle. In order to analyze lateral dynamics of the vehicle, lateral acceleration and yaw rate test data of the developed vehicle simulation model have been validated with the actual test data as shown in Figure 1.

3. DYNAMIC MODEL OF DISTURBANCE

3.1. Crosswind Model

A disturbance from the wind acting on the vehicle is validated mathematically in previous researches (Baker, 1987; Quinn *et al.*, 2001). The forces on the vehicle by crosswind are applied at the center of gravity of the vehicle in longitudinal, lateral and vertical axis. Three different moments are generated by the forces; roll, pitch and yaw represent each direction. Crosswind force and moment affect on the vehicle according to the shapes of the vehicle (Howell, 1996; Juhlin, 2008; Garry, 1994; Suzuki *et al.*, 2003). General mathematical expressions of the force and moment are represented as follows:

$$F_{CW,i} = \frac{1}{2}\rho C_{f,i} v_r^2 A \tag{1}$$

$$M_{CW,i} = C_{n,i}\frac{\rho}{2} l A v_r^2 \tag{2}$$

The crosswind coefficients on *i-th* direction, $C_{f,i}$, $C_{n,i}$ are determined by the reference shape of the vehicle. The aerodynamic coefficients have been derived from the experimental test results using flat plates (Quinn, 2001). Since the main interest of this paper is the disturbance in lateral direction, the coefficients according to the side shape of the vehicle should be described more precisely (Abe, 2009). Each coefficient of the target vehicle is shown

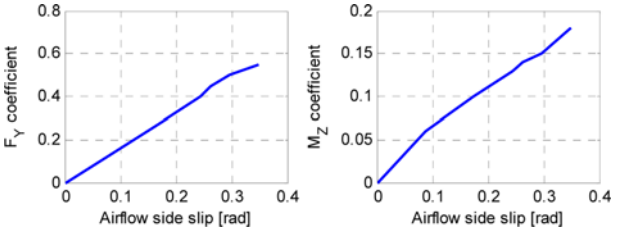

Figure 2. Lateral force, yaw moment coefficient.

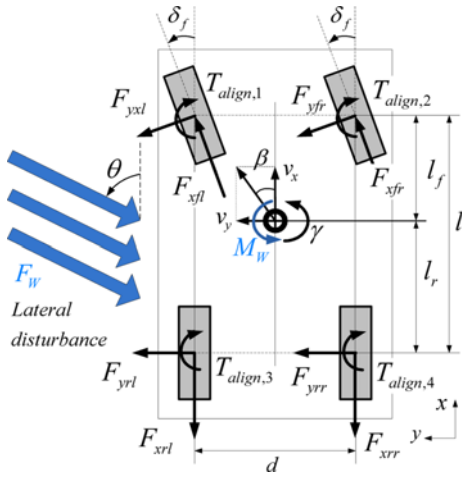

Figure 3. Total force and moment under crosswind.

in Figure 2.

An airflow side slip is an angle between the velocity of the vehicle and crosswind velocity relative to the vehicle. As the airflow side slip becomes large, lateral disturbance from the crosswind also becomes large. The total force and moment under crosswind are represented in equations (3) and (4). Figure 3 represents the schematic diagram of the disturbance.

$$\begin{aligned} m(\dot{v}_x-\gamma v_y) &= \sum F_{xri}+\sum F_{xfi}\cos\delta_f-\sum F_{yfi}\sin\delta_f-F_W\cos\theta \\ m(\dot{v}_y-\gamma v_x) &= \sum F_{yri}+\sum F_{yfi}\cos\delta_f-\sum F_{fxi}\sin\delta_f-F_W\sin\theta \end{aligned} \tag{3}$$

$$\begin{aligned} I_z\dot{\gamma} = &\sum F_{yfi}l_f\cos\delta_f-\sum F_{yri}l_r-\sum F_{xfi}l_f\sin\delta_f \\ &+\frac{d}{2}(\Delta F_{xri}+\Delta F_{fxi}\cos\delta_f)-\sum_{i=1}^{4}T_{align,i}+M_W \end{aligned} \tag{4}$$

3.2. Lateral Load by Bank Angle

A component force of gravity from a bank angle generates lateral load on a vehicle. The bank angle in the road is designed to reduce the driver's steering effort in cornering situation, but in the situation of straight driving, the bank angle of the road or unflatness from off-road can be considered as lateral disturbance to the driver. The lateral force from the bank angle is represented in Figure 4 and equations (5) and (6). The yaw dynamics of the vehicle are not disturbed by the bank angle (Rajamani, 2006). A former research has been conducted for estimating the road grade (Kim *et al.*, 2013) and bank angle using the yaw rate sensor (Chung *et al.*, 2004; You *et al.*, 2005). In this study, the total lateral force including the force generated by the bank angle is estimated using the torque sensor signal from a MDPS in order to reduce calculating load for application in real time.

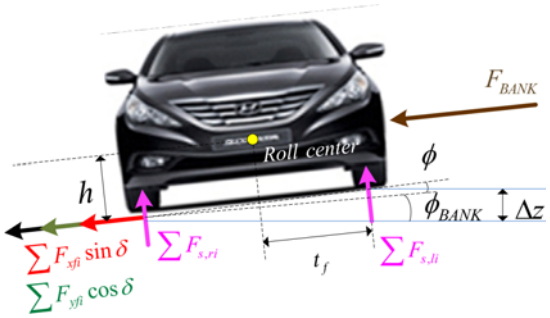

Figure 4. Total force under bank angle.

$$F_{BANK} = mg\frac{\Delta z}{2t_f} \tag{5}$$

$$\begin{aligned} \sum F_y = &F_{yfl}\cos\delta+F_{yfr}\cos\delta+F_{yrl}+F_{yrr} \\ &F_{xfl}\sin\delta+F_{xfr}\sin\delta+F_{BANK} \end{aligned} \tag{6}$$

4. LATERAL DISTURBANCE ESTIMATION

4.1. 2 DOF Bicycle Model for the Estimator

A proposed estimation algorithm has been established based on 2-degree-of freedom (DOF) linear bicycle model. The dynamics of the bicycle model under lateral load is represented in Figure 5. The total force and moment equation of the bicycle model is formed with some assumptions as follows: no slip ratio between the tire and the road, small steering angle, and the same slip angle of the left/right tire. With these assumptions, the dynamic equations can be summarized as in equations (7) and (8).

$$\sum F_y = m\cdot v_x(\dot{\beta}+\gamma) = 2F_f+2F_r+F_W \tag{7}$$

$$\sum M_z = I_z\cdot\dot{\gamma} = 2F_f\cdot l_f-2F_r\cdot l_r+M_W \tag{8}$$

Some key parameters of a bicycle model should be chosen through the simulation analysis to get the more similar behavior with a full vehicle model.

A linear tire model has been used in a bicycle model with cornering stiffness and slip angle. Tire forces of the front/rear wheel are represented with the slip angles respectively:

$$\begin{cases} \alpha_f = \delta_f-\left(\beta+\dfrac{l_f\cdot\gamma}{v_x}\right) \\ \alpha_r = -\beta+\dfrac{l_f\cdot\gamma}{v_x} \end{cases} \quad \begin{cases} F_f = C_f\alpha_f \\ F_r = C_r\alpha_r \end{cases} \tag{9}$$

4.2. Tire Self-aligning Torque Estimator

An actual tire has the property of self-alignment

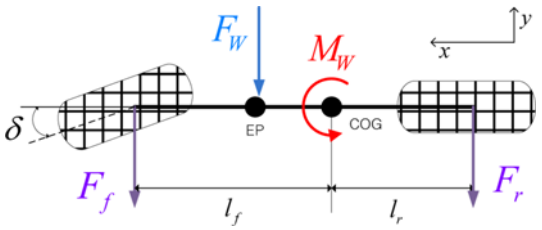

Figure 5. External force and moment on 2-DOF bicycle model.

characteristics. A slip angle is generated when the direction of the tire does not coincide with the direction of the vehicle. A cornering force of the tire makes the lateral behavior of the vehicle, and according to the magnitude of the slip angle, a cornering force is generated. In the contact area of the tire, the distance between the acting point of the cornering force and the center of the contact area is called a pneumatic trail. Because of the discordance, the self-aligning torque is generated. The magnitude of the self-aligning torque is varied according to the tire slip angle α and tire normal force Fz. The actual self-aligning torque is also affected by the pneumatic pressure of the tire and the coefficient of friction of the road. The aligning torque is decreased under the condition of the high pneumatic pressure of the tire with small contact area and the small coefficient of friction of the road for a sliding effect, but both factors are assumed to be negligible in the simulation study. The developed vehicle simulation model contains a map of the aligning torque which has been validated with the actual test data as described later.

A steering system with MDPS is described in Figure 6. The dynamics of steering system including MDPS is summarized as equation (10). In the case of straight driving with small steering angle and steering rate, the angular acceleration of the steering wheel and the friction torque can be negligible. The self-aligning torque represe-ntation with the assumptions can be rewritten as equation (11).

$$J\cdot\ddot{\theta}-N\cdot(T_{column}+T_{assist})+T_{align}+T_{friction}=0 \tag{10}$$

$$T_{align}=N\cdot(T_{column}+T_{assist}) \tag{11}$$

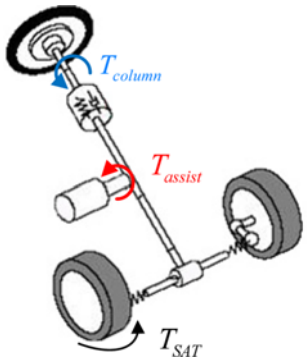

Figure 6. Steering system with MDPS.

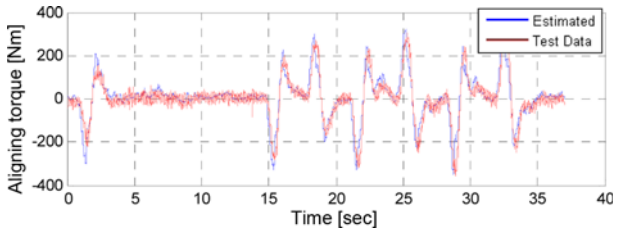

Figure 7. Aligning torque estimation.

An estimated aligning torque has been validated using test data as shown in Figure 7. The test has been conducted on dry asphalt road of high tire-road friction. The aligning torque of the test vehicle has been measured with the torque sensor within the tire, and the estimation is confirmed to be reliable even in the slalom test with large steering input.

4.3. Lateral Disturbance Estimator

A self-aligning torque varies according to a normal force and a slip angle, however, if there is little change in the normal force, the aligning torque can be assumed to be varying only with the slip angle. The aligning moment has linear characteristic in the small slip angle. Under lateral disturbance, even the heavy lateral disturbance with 15m/s crosswind speed, the aligning moment shows linear characteristic with the proportional rate of 6750~7640 *Nm/rad*.

The slip angle of the front tire is represented as in equation (12). The reactive torque applied to the steering system is the sum of the aligning torque from the both front tires. The aligning torque is represented with the tire slip angle and the proportional rate, K as given in equation (12):

$$T_{align}=2K\cdot\alpha_f=2K\delta_f-2K\left(\beta+\frac{l_f\cdot\gamma}{v_x}\right) \tag{12}$$

A Kalman filter is adopted to estimate lateral disturbance as represented in equations (13), (14), (15) and (16). Yaw rate from Electronic Stability Control (ESC) which is commonly equipped for safety, and an aligning torque estimated by MDPS module given in equation (11) have been used to form an output matrix. The state-space representation of the system is obtained from the bicycle model dynamics with the additional lateral force and moment dynamics. In the previous research conducted by Glaser *et al*. (2008), lateral wind force estimation has been proposed using the vision sensor signal for lane departure warning system. The vision sensor for lane departure warning system is less common component of the vehicle so far and it has limited usage in the bad weather. On the contrary, since MDPS is expected to be an alternative system to replace the conventional hydraulic power steering system, the torque signals from MDPS sensors are expected to be easily obtained.

The state vector of a system matrix is given as follows: $x=[\beta\ \gamma\ F_W\ M_W]^T$. The dynamics based on linear bicycle model under lateral load with steering input is represented as follows:

$$\dot{x}=Ax+B\delta_f+B_WW \tag{13}$$

$$\begin{bmatrix}\dot{\beta}\\ \dot{\gamma}\\ \dot{F}_{CW}\\ \dot{M}_{CW}\end{bmatrix}=\begin{bmatrix}-\frac{2(C_f+C_r)}{m\cdot v_x} & -1-\frac{2(l_f\cdot C_f-l_r\cdot C_r)}{m\cdot v_x^2} & \frac{1}{m\cdot v_x} & 0\\ -\frac{2(l_f\cdot C_f-l_r\cdot C_r)}{I_z} & -\frac{2(l_f^2\cdot C_f-l_r^2\cdot C_r)}{I_z\cdot v_x^2} & 0 & \frac{1}{I_z}\\ 0 & 0 & 0 & 0\\ 0 & 0 & 0 & 0\end{bmatrix}\begin{bmatrix}\beta\\ \gamma\\ F_W\\ M_W\end{bmatrix}$$

$$+\begin{bmatrix}\frac{2\cdot C_f}{m\cdot v_x}\\ \frac{2\cdot l_f\cdot C_f}{I_z}\\ 0\\ 0\end{bmatrix}\delta_f+\begin{bmatrix}0&0\\0&0\\1&0\\0&1\end{bmatrix}\begin{bmatrix}W_{F_{CW}}\\ W_{M_{CW}}\end{bmatrix}$$

Measured yaw rate γ and an estimated self-aligning torque shown in equation (12) are used to form the output matrix as:

$$y = Hx + D\delta_f + v$$

$$= \begin{bmatrix}0 & 1 & 0 & 0\\ -K & -\frac{K\cdot l_f}{v_x} & 0 & 0\end{bmatrix}\begin{bmatrix}\beta\\ \gamma\\ F_W\\ M_W\end{bmatrix}+\begin{bmatrix}0\\ K\end{bmatrix}\delta_f+\begin{bmatrix}v_\gamma\\ v_{T_{AL}}\end{bmatrix} \quad (14)$$

In the simulation study, a sequence of events occurs in discrete steps with the interval of sampling time, hence, the discrete-time Kalman filter is chosen as the estimator (Brown and Hwang, 1997). Euler discretization of equation (13) is represented as follows:

$$x(t+\Delta t) = (I + A\Delta t)x(t) + B\Delta t\,\delta_f(t) + B_W\Delta t W$$
$$= \Phi x(t) + \mathrm{E}\delta_f(t) + \Gamma W \quad (15)$$

A discrete-time Kalman filter consists of measurement update process and time propagation process represented as follows:

$$K_k = M_k H^T (HM_k H^T + V)^{-1}$$
$$\hat{x}_k = \hat{x}_k^- + K_k(z_k - H\hat{x}_k^- - D\delta_f)$$
$$P_k = (I - K_k H)M_k \quad (16)$$
$$\hat{x}_{k+1}^- = \Phi_k \hat{x}_k + \mathrm{E}\delta_{f,k}$$
$$P_{k+1}^- = \Phi_k P_k \Phi_k^T + \Gamma\, W \Gamma^T$$

The proposed estimator architecture is shown in Figure 8. The torque signals from the MDPS module have the following characteristics: 0.001Nm Sensor resolution and 0.0039sec Sensor computation delay. These sensor characteristics can be negligible to the performance of the estimator.

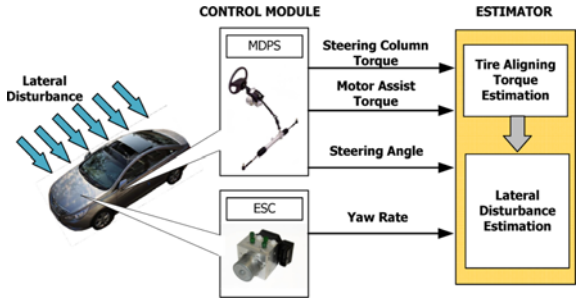

Figure 8. Estimation architecture.

5. PARAMETER UNCERTAINTIES

In real driving, nominal parameters used in the estimator vary within a certain range. In order to minimize the estimation error, the appropriate nominal parameters should be investigated. The key parameters which can affect significantly on the performance of the estimator are considered as a mass, inertia, center of gravity and tire cornering stiffness. The possible cases of the mass and inertia variation are given in Figure 9:

The center of gravity is changed along with the variation of the mass and inertia. Each additional mass causes the variation of each normal tire force, and the center of the mass can be calculated from each normal tire force with equations (17) and (18), as shown in Figure 10.

$$y = \frac{F_{z2}+F_{z4}}{F_{z1}+F_{z2}+F_{z3}+F_{z4}}t \quad (17)$$

$$x = \frac{F_{z3}+F_{z4}}{F_{z1}+F_{z2}+F_{z3}+F_{z4}}L \quad (18)$$

Vehicle yaw moment of inertia is directly related with the weight of the mass, the distance between the center of the gravity, and the mass center of the additional mass. In order to minimize the estimation error from the parameter uncertainties, five different nominal parameter

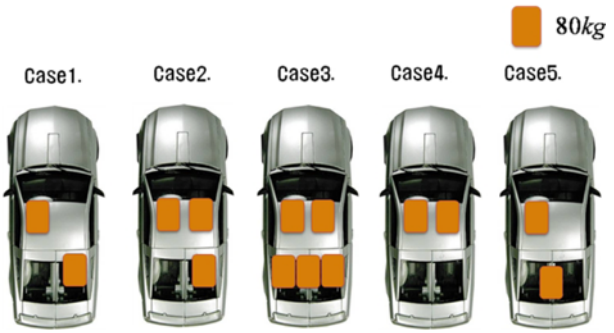

Figure 9. Mass/Inertia variation.

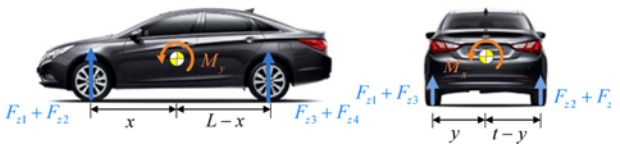

Figure 10. Center of gravity with tire normal force.

Table 1. Nominal parameter candidates.

	Est 1	Est 2	Est 3	Est 4	Est 5
Mass (kg)	1500	1600	1700	1800	1900
Inertia (kgm^2)	2800	2850	2900	2950	3000
lf (m)	1.07	1.12	1.17	1.22	1.27
lr (m)	1.725	1.625	1.625	1.575	1.525

sets are selected to be applied to the estimator. Each nominal parameter set is shown in Table 1.

The appropriate parameter set has been chosen by the mathematical simulations. The root mean square (RMS) errors of the estimated force and moment are calculated in each estimation case. The RMS errors of force and moment are used to form the error index as equation (19). Here, q_1 and q_2 are the weighting factors for force and moment respectively. The error index indicates the appropriate nominal parameters among five parameter sets in the estimation algorithm. As a result, the third parameter set shows the minimum weighted sum of RMS of the estimated force and moment as shown in Figure 11, i.e., the best nominal parameter set for the estimation algorithm.

$$J = q_1\sqrt{\frac{\sum e_f^2}{N}} + q_2\sqrt{\frac{\sum e_m^2}{N}} \tag{19}$$

Tire cornering stiffness is the characteristics of the tire, which varies according to the tire normal force. Under lateral disturbance, the load transferred to the opposite direction of the disturbance. Two distinguishable levels of lateral load are applied to the vehicle model with small steering input for straight driving. Heavy level load condition contains 15m/s speed of crosswind and -3~3deg for bank angle and 2m/s crosswind and -1~1deg bank angle for light level load. Each cornering stiffness in different load condition is compared to obtain the representative values, as shown in Figure 12. The variation of the cornering stiffness between heavy load and light load is negligible, that is, a vertical load variation in different level

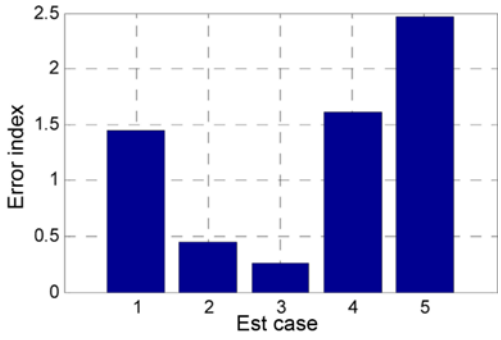

Figure 11. Error index of the parameter sets.

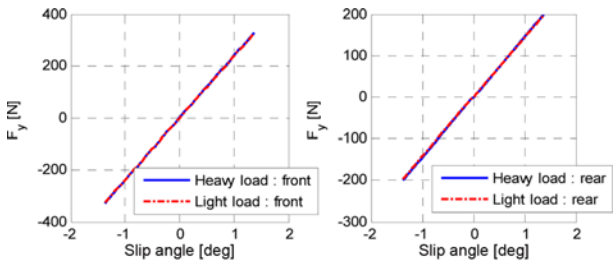

Figure 12. Cornering stiffness in heavy/light load.

of lateral load is not significant. Therefore, under lateral load condition with small steering input, constant cornering stiffness is expected to be reliable.

6. SIMULATION RESULT

Simulation results with the proposed parameters are shown in Figures 13 and 14. Each lateral load circumstance is heavy and light level of lateral disturbance respectively. Each simulation has been conducted with the small steering wheel angle, -15~15deg, for the straight driving. For both levels of lateral load, the estimator shows good performance of errors within 10%.

A proposed estimator has been evaluated with a test vehicle, Hyundai YF Sonata F-24, which parameters are shown in Table 2. The test has been conducted in the straight road under crosswind blowing from the seaside. The magnitude and direction of the lateral disturbance caused by the crosswind is hard to measure, hence, an alternative method for verification has been used. The

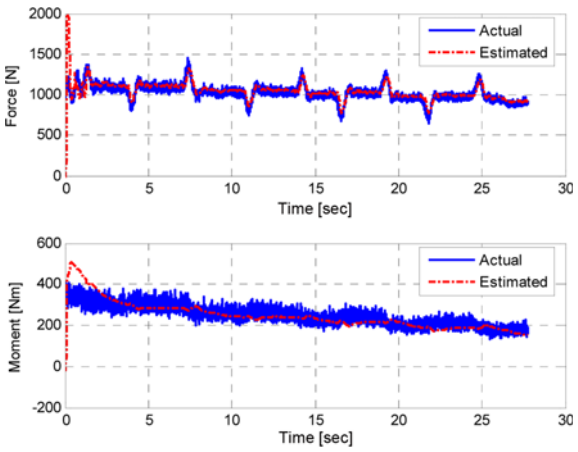

Figure 13. Lateral force and yaw moment estimation under heavy lateral load.

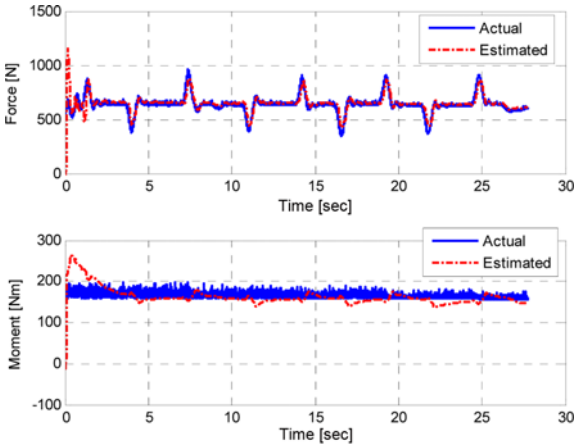

Figure 14. Lateral force and yaw moment estimation under light lateral load.

Table 2. Parameters and values of the test vehicle.

Symbol	*m*	I_z	l_f	l_r	t_f
Value	1466 kg	2744 kgm^2	1.071 m	1.724 m	1.587 m

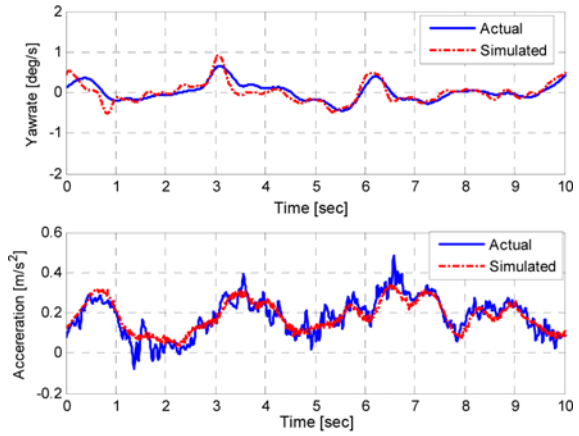

Figure 15. Simulated yaw rate and lateral acceleration and measured signals.

estimated lateral force and yaw moment using the measured signals from the test data have been applied to the simulation model, and the actual lateral and yaw behaviors in the test have been compared with the yaw rate and lateral acceleration from the simulation with the estimated lateral disturbances as shown in Figure 15. The simulated yaw rate and lateral acceleration under the estimated lateral disturbance is similar to the actual data with good accuracy.

7. CONCLUSION

In this paper, a real time lateral disturbance estimator considering parameter variation has been presented. In actual driving, crosswind and road bank angle were considered as the key factors of the lateral disturbance. The proposed estimator uses the sensor signals from an ESC, steering angle and the aligning torque estimated using MDPS torque sensors. The performance of the aligning torque estimator has been evaluated using test data obtained on dry asphalt road of high tire-road friction. Parameter variation in the actual driving is considered with mass, inertia, center of gravity and tire characteristics. The appropriate parameters are selected from the mathematical simulation in various circumstances. Simulation results of different levels of lateral disturbance have shown that vehicle lateral disturbance can be estimated by the proposed estimator with good accuracy.

ACKNOWLEDGEMENT–This work has been suppor-ted by Hyundai Mobis, SNU-IAMD, and the National Research Foundation of Korea(NRF) grant funded by the Ministry of Science, ICT & Future Planning (MSIP) (No. 2009-0083495).

REFERENCES

Abe, M. (2009). *Vehicle Handling Dynamics: Theory and Application*. 1st edn. Butterworth-Heinemann. Oxford. UK.

Baker, C. J. (1986). A simplified analysis of various types of wind-induced road vehicle accidents. *J. Wind Engineering and Industrial Aerodynamics*, **22**, 69–85.

Baker, C. J. (1987). Measures to control vehicle movement at exposed sites during windy periods. *J. Wind Engineering and Industrial Aerodynamics*, **25**, 151–161.

Brown, R. G. and Hwang, P. Y. C. (1997). *Introduction to Random Signals and Applied Kalman Filtering*. 3rd edn. Wiley. Hoboken. USA.

Chung, T., Min, K. and Yi, K. (2004). Experimental validations of vehicle lateral velocity and bank angle estimator. *Proc. KSAE*, 674–679.

Garry, K. P. (1994). *Lateral Aerodynamic Characteristics of Motor Vehicle in Transient Crosswinds*. Ph. D. Dissertation. College of Aeronautics, Department of Aerospace Science, Cranfield University.

Glaser, S., Mammar, S. and Dakhlallah, D. (2008). Lateral wind force and torque estimation for a driving assistance. *IFAC*.

Ha, J., Chung, T., Kim, J., Yi, K. and Lee, J. (2003). Validation of 3D vehicle model and driver steering model with vehicle test. *Proc. KSAE*, 676–681.

Howell, J. P. (1996). The side load distribution on a Rover 800 saloon car under crosswind conditions. *J. Wind Engineering and Industrial Aerodynamics*, **60**, 139–153.

Juhlin, M. (2008). Aerodynamic loads on buses due to crosswind gusts-on-road measurements. *Vehicle System Dynamics*, **46**, Supplement, 827–835.

Kim, I., Kim, H., Bang, J. and Huh, K. (2013). Development of estimation algorithms for vehicle's mass and road grade. *Int. J. Automotive Technology* **14**, **6**, 889–895.

Quinn, A. D., Baker, C. J. and Wright, N. G. (2001). Wind and vehicle induced forces on flat plates-Part 1: Wind induced force, **89**, 817–829.

Rajamani, R. (2006). *Vechicle Dynamics and Control*. Springer. New York.

Suzuki, M., Tanemoto, K. and Maeda, T. (2003). Aerodynamic characteristics of train/vehicle under crosswind. *J. Wind Engineering and Industrial Aerodynamics*, **91**, 209–218.

You, S., Yoo, S., Hahn, J. and Lee, K. (2005). Real-time estimation of vehicle lateral velocity and road bank angle. *Proc. KSME*, 829–835.